An Approximation of 2-D Inverse Scattering Problems From a Convex Optimization Perspective

Yangqing Liu, *Student Member, IEEE*, Shuo Han, *Member, IEEE*, Francesco Soldovieri, *Senior Member, IEEE*, and Danilo Erricolo, *Fellow, IEEE*

***Abstract*— We present a two-step strategy to solve an inverse scattering problem in 2-D geometry. The first step approximates the inverse scattering as a convex optimization problem and provides an estimation of the total field inside the domain under investigation without *a priori* knowledge or tuning parameters. In the second step, the previously estimated total field is used to reconstruct the unknown contrast permittivity, which is represented by a superposition of level-1 Haar wavelet transform basis functions. Subject to ℓ_1-norm constraints of the wavelet coefficients, a least absolute shrinkage and selection operator (LASSO) problem that searches for the global minimum of the ℓ_2-norm residual is exploited by accounting for the sparsity of the wavelet-based permittivity representation. Numerical results are presented to assess the effectiveness of the proposed formulation against objects with relatively small electric size. Finally, the approach is validated against experimental data.**

***Index Terms*— Convex optimization, CVX, Haar transform, inverse scattering, least absolute shrinkage and selection operator (LASSO), radar imaging, templates for first-order conic solver (TFOCS).**

I. Introduction

In INVERSE scattering problems, the electromagnetic, and morphological properties of targets are estimated from the scattered field [1]–[3]. Despite the relative simplicity of the sensing phenomenon, inverse electromagnetic scattering problems are characterized by challenging mathematical difficulties such as nonlinearity and ill-posedness [1], [3]–[5].

The first class of solution approaches to the quantitative inverse problem are based on iterative minimization schemes with regularizations, such as the Born iterative method (BIM) [6] and the distorted BIM [7]. The contrast source inversion method [8] is also a deterministic minimization method. Another class of approaches uses a quadratic model of the electromagnetic scattering that permits to enlarge the class of retrievable unknowns compared to the one of the linear inverse models [9], [10].

Improved reconstruction methods are present in the literature as in [11], where the unknowns are searched within the wavelet domain and the optimization problem consists of the minimization of the misfit about the data with the sparsity constraints on the wavelet coefficients. To exploit sparsity [12], wavelet transforms, such as Haar and the Daubechies wavelets, have been applied to a wide range of problems in nonlinear electromagnetic inversions [13]. Besides the deterministic approaches to solve inverse scattering problems, a further class of approaches is based on stochastic searches of the solution [1], and deep learning with neural network approaches [14].

Convex optimization problems exhibit a number of computational benefits because they are a special class of nonlinear optimizations problems [15]. First, every local optimum of a convex optimization problem is also globally optimal; this implies that convex problems can be solved using efficient local search methods (e.g., Newton's method) as opposed to expensive global methods (e.g., genetic algorithms). With modern solvers specifically designed for convex optimization, a commodity desktop computer can easily handle convex optimization problems up to 10^3 to 10^6 variables [16], depending on the problem type. Second, in many modern software packages (e.g., CVX [17], [18]) for convex optimization, users can specify convex optimization problems in high-level domain-specific languages. Finally, it is known that convex optimization problems can be solved by solving a sequence of linear systems of equations [19]. This opens the possibility to solve convex problems of very large size by leveraging existing techniques from large-scale numerical linear algebra.

In this work, we approximate the nonlinear inverse scattering problem as a convex optimization one by proposing a new inversion strategy consisting of two steps. First, we estimate the total field inside the domain of investigation by solving a convex optimization problem, which is obtained by discretizing continuous electric field integral equations by the Method of Moment [20]. The solution of the convex optimization problem can be efficiently computed using CVX [17], [18], a software package for solving generic convex optimization problems. Second, the estimated total field is exploited to formulate an inverse problem that reconstructs the dielectric permittivity and conductivity of the target from the scattered

Manuscript received September 8, 2020; revised December 11, 2020 and February 5, 2021; accepted April 29, 2021. Date of publication May 27, 2021; date of current version January 5, 2022. *(Corresponding author: Yangqing Liu.)*

Yangqing Liu and Shuo Han are with the Department of Electrical and Computer Engineering, University of Illinois Chicago, Chicago, IL 60607 USA (e-mail: yliu299@uic.edu; hanshuo@uic.edu).

Francesco Soldovieri is with the Institute for Electromagnetic Sensing of the Environment of the National Research Council of Italy, 80124 Naples, Italy (e-mail: soldovieri.f@irea.cnr.it).

Danilo Erricolo is with the Department of Electrical and Computer Engineering, University of Illinois Chicago, Chicago, IL 60607 USA, and also with the Discovery Partner Institute, Chicago, IL 60606 USA (e-mail: derric1@uic.edu).

Digital Object Identifier 10.1109/LGRS.2021.3079885

field data. To mitigate the ill-posedness of the inverse problem at the second step, we assume that the permittivity profile has a sparse representation in the wavelet domain. This regularizes the inverse problem by introducing an ℓ_1-norm penalty, which is known to promote sparsity in the Haar wavelet coefficients [11]. The resulting problem is known as the least absolute shrinkage and selection operator (LASSO) [21] problem and can be solved by the templates for first-order conic solvers (TFOCSs) [22] software package.

II. Theory

We consider the classical inverse scattering problem in 2-D geometry with the free space as background medium. The transmitting antennas are modeled as filamentary electric currents with the invariance axis orthogonal to the 2-D plane. Thus, the electric field is scalar in this TM-mode case.

Let S be the domain under investigation, and $\mathbf{r}' \in S$. We denote by $\epsilon = \epsilon' - j(\sigma/\omega\epsilon_0)$ the relative complex dielectric permittivity in S, where ϵ' and σ are the relative dielectric permittivity and electrical conductivity.

The electromagnetic scattering is governed by a pair of integral equations. The state equation accounts for the total field E_p inside the investigation domain S_n as

$$E_p + \frac{jk_0^2}{4}\sum_{n=1}^{N}(\epsilon_n - 1)E_n \int_{S_n} \mathrm{H}_0^{(2)}\left(k_0\left|\mathbf{r}_p - \mathbf{r}'_n\right|\right) \mathrm{d}S' = E_p^i \tag{1}$$

where E_p^i is the incident field at pixel p, $\mathbf{r}_p \in S$, $\mathrm{H}_0^{(2)}(\cdot)$ is the Hankel function of the second kind and order zero, and k_0 is the wavenumber in free space. The investigation domain S is discretized into N pixels, and ϵ_n is the homogeneous relative complex dielectric permittivity within the pixel n. The integral of $\mathrm{H}_0^{(2)}(\cdot)$ over a circular region S_n was evaluated in [20] as

$$\frac{jk_0^2}{4}\int_{S_n} \mathrm{H}_0^{(2)}(k_0|\mathbf{r}_p - \mathbf{r}'_n|)\,\mathrm{d}S' = \begin{cases} \dfrac{j\pi k_0 r_{\mathrm{eq}}}{2}\mathrm{H}_1^{(2)}(k_0 r_{\mathrm{eq}}) + 1, & \text{if } p = n \\ \dfrac{j\pi k_0 r_{\mathrm{eq}}}{2}\mathrm{J}_1(k_0 r_{\mathrm{eq}})\,\mathrm{H}_0^{(2)}\left(k_0\left|\mathbf{r}_p - \mathbf{r}'_n\right|\right), & \text{otherwise} \end{cases} \tag{2}$$

where r_{eq} is the equivalent radius of the discretized pixel, and $\mathrm{J}_1(\cdot)$ is the Bessel function of the first kind and first order.

The data equation describes scattered field E^s at the mth transmitter–receiver combination by

$$E_m^s = -\frac{jk_0^2}{4}\sum_{n=1}^{N}(\epsilon_n - 1)E_n \int_{S_n} \mathrm{H}_0^{(2)}\left(k_0\left|\mathbf{r}_m - \mathbf{r}'_n\right|\right) \mathrm{d}S'. \tag{3}$$

A. Approximate 2-D Inverse Scattering via Convex Optimization

A multiview/multistatic/single-frequency configuration is considered for the problem at hand. We assume N_{TX} transmitters and N_{RX} receivers encircling the investigation domain, i.e., $N_{\mathrm{TX}}N_{\mathrm{RX}}$ observations of the scattered field. Let the vector, $\epsilon_\delta = \epsilon - 1$, $\epsilon_\delta \in \mathbb{C}^N$, be the complex contrast function for N pixels, and the matrix variable $Y \in \mathbb{C}^{N\times N_{\mathrm{TX}}}$ be the total field at N pixels due to N_{TX} transmitters. These two variables allow as to write (1) and (3) as

$$A\ \mathrm{diag}(\epsilon_\delta)\, Y = D \tag{4}$$

$$Y + B\ \mathrm{diag}(\epsilon_\delta)\, Y = C \tag{5}$$

where $D \in \mathbb{C}^{N_{\mathrm{RX}}\times N_{\mathrm{TX}}}$ consists of the scattered field data E_m^s in (3). The matrices, $A \in \mathbb{C}^{N_{\mathrm{RX}}\times N}$, $B \in \mathbb{C}^{N\times N}$, and $C \in \mathbb{C}^{N\times N_{\mathrm{TX}}}$, are known once the measurement configuration and the number of pixels are fixed. Elements of A relate the scattered field collected at the n_{RX} receiver to pixel p as

$$A_{n_{\mathrm{RX}},\,p} = -\frac{j\pi k_0 r_{\mathrm{eq}}}{2}\,\mathrm{J}_1(k_0 r_{\mathrm{eq}})\,\mathrm{H}_0^{(2)}\left(k_0\left|\mathbf{r}_{n_{\mathrm{RX}}} - \mathbf{r}'_p\right|\right). \tag{6}$$

Elements of the symmetric matrix B, given in (2), rely on the relationship between pixels p and n. The matrix C accounts for the incident field radiated by a filamentary current in free space, which is expressed at pixel p for transmitter n_{TX} as

$$C_{n_{\mathrm{TX}},\,p} = -\frac{k_0^2}{4\omega\epsilon_0}\,\mathrm{H}_0^{(2)}\left(k_0\left|\mathbf{r}_{n_{\mathrm{TX}}} - \mathbf{r}'_p\right|\right). \tag{7}$$

$D_{n_{\mathrm{RX}},\,n_{\mathrm{TX}}}$ is the scattered field data at receiver n_{RX} due to transmitter n_{TX}.

Equation (4) contains data of the problem, i.e., the scattered field, whereas (5) accounts for the total field within the investigation domain. Therefore, a nonconvex optimization problem can be reformulated from (4) and (5) as

$$\min_{Y,\,\epsilon_\delta}\ \|A\ \mathrm{diag}(\epsilon_\delta)\, Y - D\|_2 \quad \text{s.t. } Y + B\ \mathrm{diag}(\epsilon_\delta)\, Y = C. \tag{8}$$

To approximate the nonconvex problem (8), we substitute $\mathrm{diag}(\epsilon_\delta)\, Y$ with a new optimization variable, $Z \in \mathbb{C}^{N\times N_{\mathrm{TX}}}$

$$\min_{Y,\,Z}\ \|A\, Z - D\|_2 \quad \text{s.t. } Y + B\, Z = C. \tag{9}$$

The objective function is a Euclidean norm of an affine function, and the constraint is also affine; therefore, this optimization problem is convex [15]. This convex optimization problem does not require picking appropriate regularization parameters. With CVX, optimal solutions, $\hat{Y}$ and $\hat{Z}$, of our stated convex optimization problem are easily obtained. Equation (9) relaxes the nonlinear inverse problem and considers the equivalent currents and the total field inside the investigation domain as separate optimization variables. Due to the nonuniqueness of optimal solutions, CVX would arbitrarily retrieves one solution from the set of optimal solutions and varying constraints do not affect the set of optimal solutions. For any Z, there exists Y such that the constraint is satisfied. The inverse source problem, the estimation of Z, is affected by the inherent nonuniqueness issue as discussed in [23] and [24] that we are trying to estimate a function of spatial variables (defined over a 2-D investigation domain) by exploiting the knowledge of the scattered field on a line (1-D domain).

The weakness of approximating the original problem as a convex optimization problem is the absence of the nonconvex constraint of $Z = \mathrm{diag}(\epsilon_\delta)\, Y$. Consequently, solution $\hat{Z}$ returned by CVX cannot be expressed as the multiplication of a diagonal matrix and the solution $\hat{Y}$. To estimate the permittivity contrast ϵ_δ, we only use the estimated total field, $\hat{Y}$, and adopt a LASSO problem at the second step.

B. Linear Inversions in the Wavelet Domain

Equation (4) can be reformulated to determine the unknown permittivity contrast ϵ_δ through $\hat{Y}$ returned at the first step.

We separate real and imaginary parts of matrices in (4) so that in the real domain

$$\begin{bmatrix} \Re\mathcal{O} & \Im\mathcal{O} \\ \Im\mathcal{O} & -\Re\mathcal{O} \end{bmatrix} \begin{bmatrix} \Re\epsilon_\delta \\ -\Im\epsilon_\delta \end{bmatrix} = \begin{bmatrix} \Re D_{*,\,1} \\ \vdots \\ \Re D_{*,\,N_{\mathrm{TX}}} \\ \Im D_{*,\,1} \\ \vdots \\ \Im D_{*,\,N_{\mathrm{TX}}} \end{bmatrix} \tag{10}$$

where the linear complex operator $\mathcal{O}$ is

$$\mathcal{O} = \begin{bmatrix} A_{1,\,*} \circ \hat{Y}_{*,\,1} \\ \vdots \\ A_{N_{\mathrm{RX}},\,*} \circ \hat{Y}_{*,\,1} \\ A_{1,\,*} \circ \hat{Y}_{*,\,2} \\ \vdots \\ A_{N_{\mathrm{RX}},\,*} \circ \hat{Y}_{*,\,N_{\mathrm{TX}}} \end{bmatrix} \tag{11}$$

with element-wise multiplication symbol $\circ$, and all elements in a specific row or column omitted by $*$. Apparently, (10) shows a linear form

$$\mathcal{L}\, m = d \tag{12}$$

through a linear operator, $\mathcal{L} \in \mathbb{R}^{2N_{\mathrm{TX}}N_{\mathrm{RX}} \times 2N}$, between the data, $d \in \mathbb{R}^{2N_{\mathrm{TX}}N_{\mathrm{RX}}}$, and the unknown model, $m \in \mathbb{R}^{2N}_{\geq 0}$.

To tackle the ill-posedness of the inversion of the linear operator $\mathcal{L}$, we apply an ℓ_1-norm based regularization term. When the permittivity profile either is smooth or contains limited sharp features, the unknown permittivity function can be projected in the wavelet domain. Therefore, the model m can be unraveled by a linear inverse wavelet transform operator $\mathcal{W}^{-1}$ and the wavelet coefficients w as $m = \mathcal{W}^{-1}w$. To improve sparsity, we penalize the misfit between the data and the proposed model with sparse constraints in the wavelet domain as the LASSO problem [21]

$$\begin{aligned} &\min_{w} \ \frac{1}{2}\|\mathcal{L}\mathcal{W}^{-1}w - d\|_2^2 \\ &\text{s.t. } \|w\|_1 \leq \gamma\,. \end{aligned} \tag{13}$$

The parameter γ controls the sparsity of the solution for w, where the value of γ increases when we consider contrast functions with higher frequency content. Therefore, γ is the maximum value that forces the solution $\|w\|_1$ returned by TFOCS at each iteration to decrease for sparsity. The feasible initial point of w is set as $w_0 = \mathbf{0}$.

III. Numerical Results and Analysis

In this section, we assess the proposed approach by considering both simulated and experimental data. For the synthetic cases, the investigation domain S is divided into finer pixels (144×144) in the forward model compared to the ones used in the inverse model (50×50). The fine grid in the forward model ensures more accurate numerical computations of the scattered field and avoids committing the inverse crime. Eight transmitters and 36 receivers give rise to 288 scattered field data. Transmitters and receivers are located evenly along the circle at 1.5 times the radius of the circular investigation domain S.

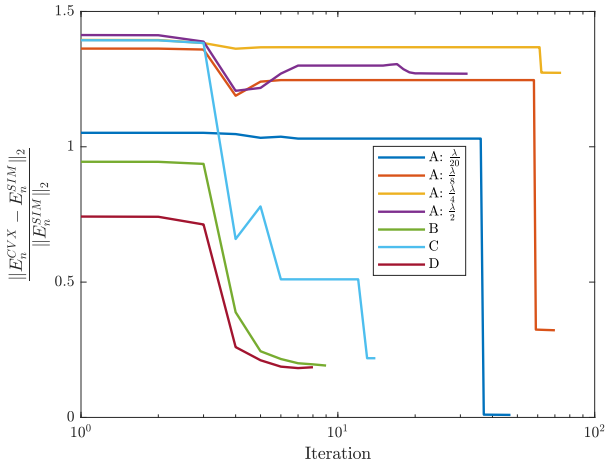

Fig. 1. Relative error of total field within the investigation domain returned by CVX at each iteration compared with exact total field.

TABLE I

ℓ-2 Norm Relative Error in Percentage

	A: $\frac{\lambda}{20}$	A: $\frac{\lambda}{8}$	A: $\frac{\lambda}{4}$	A: $\frac{\lambda}{2}$	B	C	D
$\frac{\|E_n^{CVX} - E_n^{SIM}\|_2}{\|E_n^{SIM}\|_2}\%$	0.93	32.21	127.3	127	19.16	21.87	18.55
$\frac{\|\epsilon^{CVX} - \epsilon\|_2}{\|\epsilon\|_2}\%$	2.43	27.27	93.25	82.7	5.24	16.98	23.68
$\frac{\|E_n^{BIM} - E_n^{SIM}\|_2}{\|E_n^{SIM}\|_2}\%$	1.23	109.6	147	128.8			
$\frac{\|\epsilon^{BIM} - \epsilon\|_2}{\|\epsilon\|_2}\%$	9.27	80.13	87.4	90.71			

The SDPT3 solver implementing a particular variant of interior-point methods, and called by CVX, costs less than 2 min with an Intel Core i7-8700 CPU and 16 GB of RAM for this moderate size problem. In TFOCS, the computation time is within seconds. Overall, it is slower than BIM.

We present results and error analysis for these numerical data: 1) a homogeneous cylinder compared with BIM; 2) a sine-shaped distribution; 3) a layered cylinder; and 4) an L-shaped cylinder. For cases 2–4, we add the white Gaussian noise $\tilde{N} \sim \mathcal{N}(0, \sigma^2/2)$ (σ is the variance, not the symbol of conductivity) to the real and imaginary parts of the scattered field data $\tilde{S}$ proportionally. The signal-to-noise ratio is defined as SNR $= 10\log[\mathrm{Power}(\tilde{S})/\sigma^2]$ and set to be 20 dB. Finally, case 5) is concerned with experimental data for two high-density polyethylene (HDPE) cylinders and the results of the proposed approach are compared with the ones of a quadratic forward model.

Relative errors of reconstructed total field returned by CVX at each iteration is shown in Fig. 1. For noisy cases (2–4), CVX converges faster. All the relative errors with respect to simulated results are listed in Table I.

1. Lossless Homogeneous Cylinder: $\epsilon = 11$

To test the effectiveness of CVX, we consider a homogeneous cylinder with permittivity $\epsilon = 11$. First, we follow the case of Fig. 6 in [6] of a circular cylinder with a radius of $\lambda/20$. In BIM, the total field within the cylinder E_n^{BIM} is achieved after 14 iterations with relative residual error less than 10^{-4}. The regularization method for the inversion is

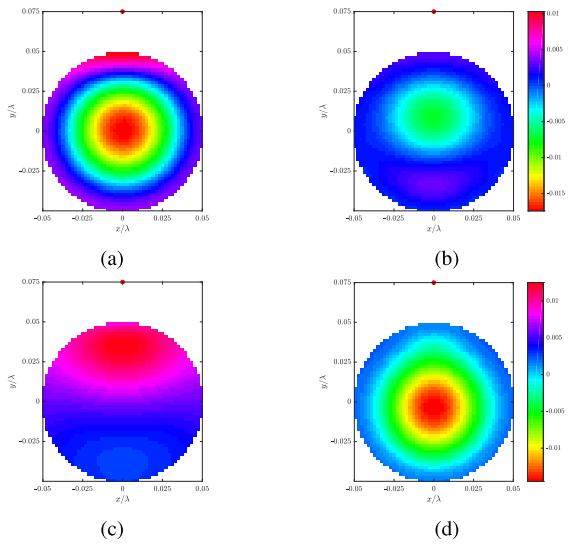

Fig. 2. Electric field relative error within the cylinder with $\epsilon = 11$: (a) $\Re\delta^{\text{BIM}}$. (b) $\Re\delta^{\text{CVX}}$. (c) $\Im\delta^{\text{BIM}}$. (d) $\Im\delta^{\text{CVX}}$. The red dot at $(0, 0.075\lambda)$ shows the location of the transmitter. Results on the same row share the colorbar on the right.

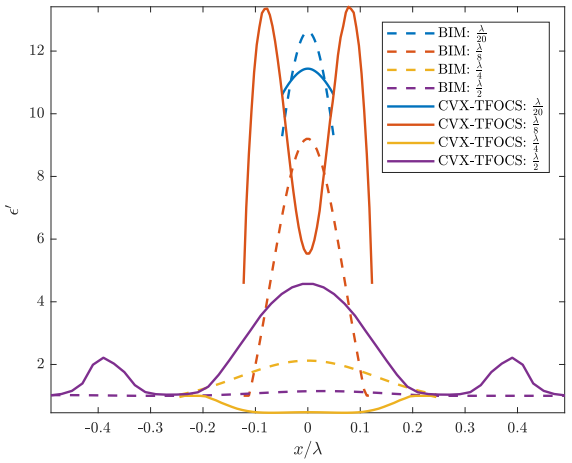

Fig. 3. Real part of permittivity reconstructed along $y = 0$ by BIM and CVX-TFOCS for a circular cylinder with permittivity 11 with varying radius, $\lambda/20$, $\lambda/8$, $\lambda/4$, and $\lambda/2$.

the algebraic reconstruction technique [25], instead of the Tikhonov regularization in [6]. The total field estimated by proposed convex optimization method is E_n^{CVX}. Fig. 2 shows the relative complex error for the total field

$$\delta^{\text{BIM, CVX}} = \frac{E_n^{\text{Simulation}} - E_n^{\text{BIM, CVX}}}{\left|E_n^{\text{Simulation}}\right|} \tag{14}$$

at each pixel of the investigation domain, when the transmitter is located at $(0, 1.5\lambda/20)$. Neither approximations nor *a priori* knowledge are used, but CVX attains a better reconstruction of the total field, especially for the real part of E_n.

The permittivity estimated along the slice of $y = 0$ by BIM and CVX-TFOCS is shown in Fig. 3. For the cylinder with a radius of $\lambda/20$, CVX-TFOCS yields less variance than BIM. Due to more accurate estimates of E_n by CVX and the exploitation of the sparse nature of a homogeneous permittivity distribution (in terms of wavelet representation), the LASSO solution enables a cleaner and more uniform reconstruction. Also, it has been observed that a good performance of the proposed approach also for even larger value of relative dielectric permittivity: $((\|E_n^{\text{CVX}} - E_n^{\text{SIM}}\|_2)/(\|E_n^{\text{SIM}}\|_2)) = 1.08\%$ for $\epsilon = 15$, 0.74% for $\epsilon = 20$, and 9.8% for $\epsilon = 40$.

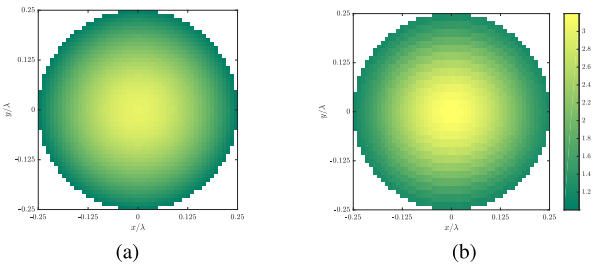

Fig. 4. Real part of permittivity within a sine-shaped permittivity distribution with maximum $\epsilon = 3$: (a) actual. (b) Reconstructed with a 20-dB SNR. Results share the colorbar on the right.

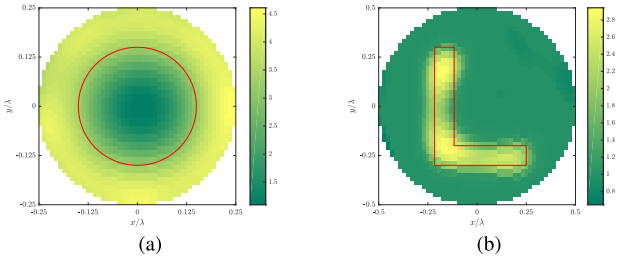

Fig. 5. Reconstructed permittivity: (a) layered cylinder, the red line indicates the actual boundary between the outer layer with $\epsilon = 4$ and the inner layer with $\epsilon = 2$. (b) L-shaped plexiglass with $\epsilon = 2.6$.

After, we assess the performance of CVX with larger objects, such as radius of $\lambda/8$, $\lambda/4$, and $\lambda/2$. Based on the discretization rule in [20], with 50×50 pixels, the edge dimension of each cell for an object with the radius $\lambda/2$ is $\lambda/50$, which does not exceed the criterion $0.2/\sqrt{11}\lambda$. Table I shows, in this case, the larger extent of the targets entails a worse quality of approximation of the total field, which leads to worse permittivity reconstruction.

2. Sine-Shaped Distribution With a 20-dB SNR

A sine-shaped permittivity distribution with maximum equal to 3 at $(0, 0)$ and the minimum equal to 1 at the edge of the circular domain with radius of $\lambda/4$ is considered. Fig. 4(b) shows the reconstructed permittivity. With noisy data, overall, the reconstructed permittivity is larger compared to the actual object in Fig. 4(a).

3. Layered Distribution With a 20-dB SNR

We consider a lossless layered cylinder, where the outer layer has permittivity $\epsilon = 4$ and the inner layer has permittivity $\epsilon = 2$. The radius of the outer layer is 0.25λ, and the radius of the inner layer is 0.15λ. Fig. 5(a) shows the reconstructed permittivity. The homogeneous spatial behavior and the permittivity value for the outer layer are well estimated, whereas there is a smoothly varying distribution for the inner layer.

4. L-Shaped Plexiglass With a 20-dB SNR

The L-shaped plexiglass with $\epsilon = 2.6$ is placed in the investigation domain of radius $\lambda/2$. Fig. 5(b) shows that the L-shape is clearly identified and that the remaining area of the investigation domain has a clean $\epsilon = 1$ almost everywhere.

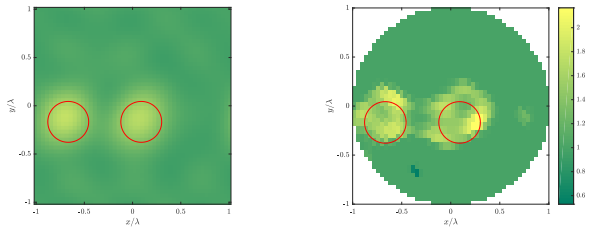

(a) (b)

Fig. 6. Reconstructed permittivity of two HDPE cylinders with $\epsilon = 2.26$: (a) quadratic model. (b) CVX-TFOCS. The red circles indicate the contour of the original cylinders. Results share the colorbar on the right.

5. Two HDPE Cylinders

We apply the proposed method to the experimental data presented in [9]. Fifteen transmitter locations were uniformly assigned along an arc of 280° with a radius of 0.432 m; 80 receiver locations were along a full circular orbit of radius 0.328 m. The transmitter and the receiver were log-periodic antennas (Ramsey Model No. LPY26) at 5 GHz. Two HDPE cylinders with a relative permittivity $\epsilon = 2.26$ are located in the domain of investigation with radius λ. The cylinders have a radius of 0.0127 m (0.21 λ) and the minimal distance between them is 0.02 m (0.33 λ). First, reconstructed permittivity is shown in Fig. 6(a) when a quadratic inverse model in [9] is used. The boundaries are smooth and the maximum permittivity is 1.7823. Fig. 6(b) presents the reconstructed permittivity by CVX-TFOCS. Two detected targets have a more accurate permittivity and most of the background area has a correctly estimated value of permittivity $\epsilon = 1$.

IV. Conclusion

We proposed a two-step strategy based on a convex optimization scheme and a LASSO scheme in the wavelet domain for solving an inverse scattering problem. After, we present a validation of the method with both simulated and experimental data. Without *a priori* knowledge or tuning regularization parameters, CVX estimates total field information well for objects with relatively small electric size and shows robustness when noise is present. Future developments should analyze theoretically the performance in the case of larger investigation domains [26] and propose more tractable constraints on this optimization problem.

Acknowledgment

The authors would like to thank Daniela Tuninetti for valuable discussions, Tadahiro Negishi and Vittorio Picco for providing the experimental data and the code about quadratic model used in Section III-E.

References

[1] M. Pastorino, *Microwave Imaging* (Microwave and Optical Engineering). Hoboken, NJ, USA: Wiley, 2010.

[2] L. Lo Monte, D. Erricolo, F. Soldovieri, and M. C. Wicks, "Radio frequency tomography for tunnel detection," *IEEE Trans. Geosci. Remote Sens.*, vol. 48, no. 3, pp. 1128–1137, Mar. 2010.

[3] R. Solimene, I. Catapano, G. Gennarelli, A. Cuccaro, A. Dell'Aversano, and F. Soldovieri, "SAR imaging algorithms and some unconventional applications: A unified mathematical overview," *IEEE Signal Process. Mag.*, vol. 31, no. 4, pp. 90–98, Jul. 2014.

[4] M. Bertero, *Introduction to Inverse Probelms Imaging*. Abingdon, U.K.: Taylor & Francis, 1998.

[5] M. Ambrosanio, M. T. Bevacqua, T. Isernia, and V. Pascazio, "The tomographic approach to ground-penetrating radar for underground exploration and monitoring: A more user-friendly and unconventional method for subsurface investigation," *IEEE Signal Process. Mag.*, vol. 36, no. 4, pp. 62–73, Jul. 2019.

[6] Y. M. Wang and W. C. Chew, "An iterative solution of the two-dimensional electromagnetic inverse scattering problem," *Int. J. Imag. Syst. Technol.*, vol. 1, no. 1, pp. 100–108, 1989.

[7] W. C. Chew and Y. M. Wang, "Reconstruction of two-dimensional permittivity distribution using the distorted born iterative method," *IEEE Trans. Med. Imag.*, vol. 9, no. 2, pp. 218–225, Jun. 1990.

[8] P. M. van den Berg and A. Abubakar, "Contrast source inversion method: State of art," *Prog. Electromagn. Res.*, vol. 34, pp. 189–218, Feb. 2001.

[9] V. Picco, G. Gennarelli, T. Negishi, F. Soldovieri, and D. Erricolo, "Experimental validation of the quadratic forward model for RF tomography," *IEEE Geosci. Remote Sens. Lett.*, vol. 12, no. 7, pp. 1461–1465, Jul. 2015.

[10] R. Pierri, F. Soldovieri, A. Liseno, and F. De Blasio, "Dielectric profiles reconstruction via the quadratic approach in 2-D geometry from multifrequency and multifrequency/multiview data," *IEEE Trans. Geosci. Remote Sens.*, vol. 40, no. 12, pp. 2709–2718, Dec. 2002.

[11] M. T. Bevacqua, L. Crocco, L. D. Donato, and T. Isernia, "Nonlinear inverse scattering via sparsity regularized contrast source inversion," *IEEE Trans. Comput. Imag.*, vol. 3, no. 2, pp. 296–304, Jun. 2017.

[12] N. Anselmi, M. Salucci, G. Oliveri, and A. Massa, "Wavelet-based compressive imaging of sparse targets," *IEEE Trans. Antennas Propag.*, vol. 63, no. 11, pp. 4889–4900, Nov. 2015.

[13] A. Abubakar, T. M. Habashy, Y. Lin, and M. Li, "A model-compression scheme for nonlinear electromagnetic inversions," *Geophysics*, vol. 77, no. 5, pp. E379–E389, Sep. 2012.

[14] L. Li, L. G. Wang, F. L. Teixeira, C. Liu, A. Nehorai, and T. J. Cui, "DeepNIS: Deep neural network for nonlinear electromagnetic inverse scattering," *IEEE Trans. Antennas Propag.*, vol. 67, no. 3, pp. 1819–1825, Mar. 2019.

[15] S. Boyd and L. Vandenberghe, *Convex Optimization*. Cambridge, U.K.: Cambridge Univ. Press, 2004.

[16] H. Mittelmann. *Benchmarks for Optimization Software*. Accessed: May 21, 2021. [Online]. Available: http://plato.asu.edu/bench.html

[17] M. Grant and S. Boyd. (Mar. 2014). *CVX: MATLAB Software for Disciplined Convex Programming, Version 2.1*. [Online]. Available: http://cvxr.com/cvx

[18] M. C. Grant and S. P. Boyd, "Graph implementations for nonsmooth convex programs," in *Recent Advances in Learning and Control* (Lecture Notes in Control and Information Sciences), vol. 371, V. D. Blondel, S. P. Boyd, and H. Kimura, Eds. London, U.K.: Springer, 2008. [Online]. Available: https://link.springer.com/chapter/10.1007%2F978-1-84800-155-8_7, doi: 10.1007/978-1-84800-155-8_7.

[19] S. J. Wright, *Primal-Dual Interior-Point Methods*. Philadelphia, PA, USA: SIAM, 1997.

[20] J. Richmond, "Scattering by a dielectric cylinder of arbitrary cross section shape," *IEEE Trans. Antennas Propag.*, vol. AP-13, no. 3, pp. 334–341, May 1965.

[21] R. Tibshirani, "Regression shrinkage and selection via the lasso," *J. Roy. Stat. Soc., Ser. B Methodol.*, vol. 58, no. 1, pp. 267–288, Jan. 1996.

[22] S. R. Becker, E. J. Candès, and M. C. Grant, "Templates for convex cone problems with applications to sparse signal recovery," *Math. Program. Comput.*, vol. 3, no. 3, p. 165, 2011.

[23] A. J. Devaney, "Fundamental limitations in inverse source and scattering problems in NDE," J. Devaney Associates, Ridgefield, CT, USA, 1986. [Online]. Available: https://core.ac.uk/download/pdf/38895098.pdf

[24] W. C. Chew, Y. Wang, G. Otto, D. Lesselier, and J.-C. Bolomey, "On the inverse source method of solving inverse scattering problems," *Inverse Problems*, vol. 10, no. 3, p. 547, 1994.

[25] V. Picco, T. Negishi, S. Nishikata, D. Spitzer, and D. Erricolo, "RF tomography in free space: Experimental validation of the forward model and an inversion algorithm based on the algebraic reconstruction technique," *Int. J. Antennas Propag.*, vol. 2013, pp. 1–9, Dec. 2013, doi: 10.1155/2013/528347.

[26] W. C. Chew, Y. M. Wang, G. Otto, D. Lesselier, and J. C. Bolomey, "On the inverse source method of solving inverse scattering problems," *Inverse Problems*, vol. 10, no. 3, pp. 547–553, Jun. 1994.